Acoustic Wave Formation from Particulates Irradiated by a Laser Beam

Michael M. Tilleman*
Science Research Laboratory, Inc., Somerville, Massachusetts
and
Shmuel Eidelman*
Science Applications International Corporation, McLean, Virginia

In the present study, an analysis of acoustic waves emanating from an ensemble of particulates suspended in air that absorb laser radiation is given. A microphone is assumed to detect these acoustic waves. We predict the acquired signal waveform and show that its amplitude is proportional to both the particulate absorptivity and density. A calculation of a test case in which each particulate is assumed to absorb 0.05 erg of a pulsed laser energy emitted by a laser beam with a diameter of 3.5 cm, in a test cell having a length of 24 cm, and with a microphone placed 7.5 cm from the beam axis is presented. The predicted signal-to-noise ratio for the considered setup is 30,000, using commercially available microphones.

Nomenclature

c = speed of sound
E = energy
f = directivity response function
H = microphone response function
k = acoustic wave number
N = number of particles
P,P_0 = Fourier transforms of the ensemble and individual waves, respectively
P_{ac} = accoustic pressure signal
p = pressure
p_0 = pressure function of acoustic wave
r = radial coordinate
r_i,r_{ii} = pointing vectors from the observer to the ith wave leading and trailing edge, respectively
r_{ref} = reference distance from source
t = time
v = gas flow velocity
α = angle between normal to the observer plane and line from source to observer
γ = specific heats ratio
θ = unit step function
λ = acoustic wavelength
ω = radian frequency
ρ = gas density

I. Introduction

A STUDY evaluating the feasibility of measuring the density of particles suspended in a gas and their absorption of radiation by optoacoustic means is presented. The optoacoustic technique comprises a pulsed laser that heats a sample medium enclosed in a test cell and acoustic detectors, such as microphones, that detect the resulting pressures waves.[1] The interest in the implementation of such a technique is in the area of combustion engineering,[2] as well as in environmental research, meteorology, and defense.[3] Aerosol particle absorption and density affect the global heat balance and climate as a result of control of solar heating. Finally, aerosols absorb high-power laser radiation propagating through the atmosphere. A particular advantage of an optoacoustic measurement over optical techniques is in its independence of the cleanliness and alignment requirements, typical of an optical apparatus.

The method considered in this study is one in which, by irradiating a population of suspended particulates in gas with an intense pulsed laser beam of a typical pulsed duration of 1 μs, resulting pressure waves are observed. The amount of energy absorbed by a single particle is a function of its size and composition. In the case of a spherical particle having a diameter of the order of the irradiating laser wavelength, the Mie theory details quantitatively the amounts of absorbed and scattered energy.[4] The absorbed energy heats up the particle. Under the condition of strong heating, shock or blast waves emanate from the particle. Because these shock waves are spherical, they decay rapidly. After some distance from the particle origin, the waves attenuate to acoustic waves. In the present study, we consider suspended particles that absorb a finite amount of energy. The absorbed energy is deposited into the surrounding air immediately after the illuminating laser pulse has ended. It will be shown that the amplitude and waveform of the resulting acoustic waves are a function of the absorbed energy only and are independent of the particle size and material (these parameters, however, are important in determining the amount of the laser energy absorbed in the particle). Then, an ensemble of such waves originating from many randomly positioned particles will be calculated, forming an ensemble acoustic wave that contains frequency components detectable by acoustic sensors. The detectable ensemble signal will be shown to be typical of the particles' number density and invariant of the individual particles' position in space. The gas in which the particulates are suspended is assumed to be nonabsorptive of the laser energy. In the present study, we have devised an algorithm calculating the following stages of the diagnostic technique:

1) Direct simulation of the spherical shock waves produced by the heating particulate in air and their eventual decay to acoustic waves.

Presented as Paper 88-0184 at the AIAA 26th Aerospace Sciences Meeting, Reno, NV, Jan. 11-14, 1988; received Feb. 5, 1988; revision received Jan. 5, 1989.

*Senior Research Scientist. Member AIAA.

2) Interference between a randomly distributed particulates ensemble of acoustic waves at an observer position.

3) Fourier analysis of the ensemble interference wave and its convolution with a real acoustic sensor response characteristic.

II. Numerical Simulation of the Blast Wave Attenuation

When the particle is abruptly heated by the high-energy laser beam, high-temperature gas and very hot particle debris are concentrated in a small finite volume around the original particle location. This energy immediately begins to transfer to the surrounding air in the close vicinity to the high-energy volume. A strong shock wave is formed that starts to propagate outward from the high-energy volume.

We are interested in the acoustic signature of the initial blast wave. It is assumed that initially the blast wave is strong, and that its attenuation to an acoustic wave takes place at a distance 10 times larger than the radius of the region of initial energy release. It has previously been shown[5-7] that, at that distance, the details of the dynamics of the energy volume are not important and that the wave propagation depends only on the amount of energy released in the initial volume.

We assume that, at the time $t = 0$, the released energy from a finite spherical volume of air equal to the size of the absorbing particulate is equal to the laser energy absorbed. From that point on, the propagation of the resulting blast wave can be accurately simulated by the following set of Euler equations in spherical coordinates:

Conservation of mass:

$$\frac{\partial \rho}{\partial t} = \frac{1}{r^2}\frac{\partial (r^2 v \rho)}{\partial r} \tag{1}$$

Conservation of momentum:

$$\frac{\partial \rho v}{\partial t} = -\frac{1}{r^2}\frac{\partial (r^2 \rho v^2)}{\partial r} - \frac{\partial p}{\partial r} \tag{2}$$

Conservation of energy:

$$\frac{\partial E}{\partial t} = -\frac{1}{r^2}\frac{\partial (r^2 E v)}{\partial r} - \frac{1}{r^2}\frac{\partial (r^2 p v)}{\partial r} \tag{3}$$

where

$$E = \frac{p}{\gamma - 1} + \frac{1}{2}\rho v^2$$

For the set of hyperbolic partial differential equations (1-3), we will solve a Cauchy problem with the following initial conditions at the time $t = 0$.

In the region bordered by r_0,

$$E = E_0, \qquad \rho = \rho_0, \qquad v = 0 \tag{4a}$$

In the surrounding air,

$$E = E_a, \qquad \rho = \rho_a, \qquad v = 0 \tag{4b}$$

where the subscript 0 represents conditions in the high-energy area, and subscript a indicates conditions in the ambient air surrounding this area.

The system of Eqs. (1-3) with the boundary conditions (4a) and (4b) was solved numerically using the flux-corrected transport (FCT) method developed by Boris and Book.[8] The explicit, low-phase-error FCT algorithm was used (code JPBFCT) in order to ensure high accuracy of the blast waves and acoustic wave simulations. This code has been tested extensively for shock, blast, detonation, fluid instability, and beam-generated turbulence numerical modeling.[9]

Test Case

In order to verify our assumption that the acoustic stage of the solution is independent of the size of the high-energy region or the slow peculiarities of the initial disturbance, we have simulated the following two cases in which a laser energy of 0.05 erg is absorbed. The laser and particulate parameters that determine the amount of absorbed energy are given in the Appendix.

Case 1

The energy density in the high-energy region is 1200 J/cm^3. The high-energy region is contained in a spherical volume with a radius of $r_0 = 1$ μm. This case is simulated on a computational grid with 500 grid points, with the grid size at the center of symmetry $\Delta r = 0.1$ μm. In order to extend the size of the computational domain to 500 μm, this grid is stretched after point 150 by 1.2 percent for every grid point. The ambient air is at conditions $p = 1$, 0.13×10^5 Pa, $\rho = 1.2 \times 10^3$ g/cm^3.

Case 2

The energy density in the high-energy region is 1.2 J/cm^3, and the average density of the medium in this region is $\rho_0 = 1.2 \times 10^{-3}$ g/cm^3. The high-energy region is contained in a spherical volume with a radius of $r_0 = 10$ μm. This volume is 1000 times larger than the high-energy region volume in case 1. This ensures equality between total energies contained in the initial high-energy volume for cases 1 and 2. Case 2 is simulated on a computational grid, with evenly spaced grid points having $\Delta r = 1$ μm at the center of symmetry up to the point 350, and gradually stretching by 1.5 percent thereafter. The ambient air has the same parameters as in case 1.

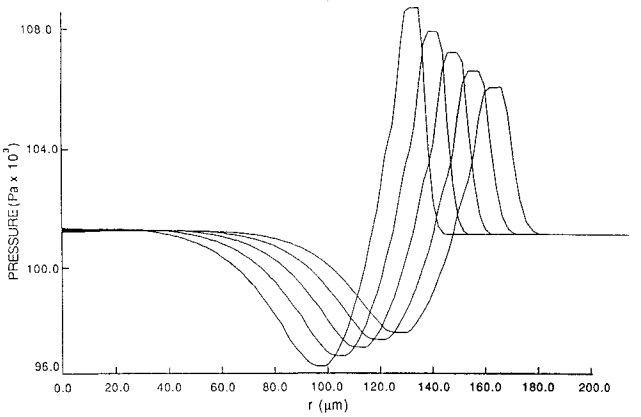

Fig. 1 Acoustic waves developing from shock waves generated by a particle of 1-μm radius that absorbed energy of 0.05 erg.

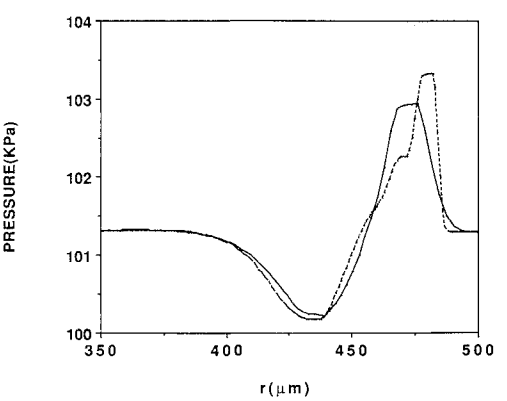

Fig. 2 Comparison of acoustic waves due to absorbing an energy of 0.05 erg by a particle with a radius of 1 μm, designated by a solid line; and 10 μm, designated by a broken line.

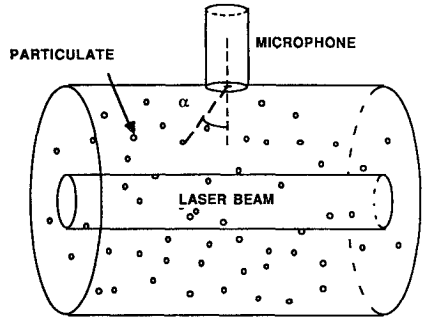

Fig. 3 Schematic of the optoacoustic measurement setup.

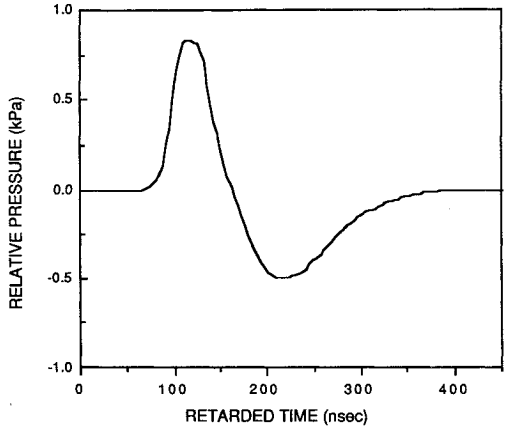

Fig. 4 Waveform of an acoustic wave emanating from a single source, at a distance of 1 cm from the wave source, from energy absorption of 0.04 erg. The abscissa is given in terms of retarded time, and the ordinate is relative to the ambient pressure.

The results for the simulation of case 1 are presented in Fig. 1 in the form of the graphs of pressure distribution for a specific time of the simulation. At the time represented in Fig. 1, the radius of the waves is nearly 200 times the initial radius of the high-energy region. The acoustic waves shown in Fig. 1 are fully developed and have a wavelength of $\sim 100\ \mu$m.

In Fig. 2, we compare the acoustic wave obtained from simulating case 1 (solid line) with the acoustic wave obtained by solving case 2 (dot-dashed line) at an equal radial location. The wavelengths of the two waves shown in Fig. 2 are within ~ 5 percent accuracy. The small disagreement in the maximum values in the positive part of the acoustic wave can be explained by the differences in conditions for the numerical integration, such as grid size and number of integration steps. For instance, simulation of the case 1 shown in Fig. 2 is obtained after 25,000 integration steps (because of the need to comply with CFL criteria on the stretched grid), and case 2 takes only 4000 steps to integrate. We can conclude from the comparison that, at the large distances from the source, the blast waves acoustic signature will depend only on the amount of energy absorbed by the aerosols.

III. Acoustic Wave Ensemble

Once the spherical wave generated by the heated particle has reached the form of an acoustic wave, its further propagation only attenuates its amplitude reciprocally to the radial distance, but its spectral content remains unchanged. The distance at which the acoustic wave conditions are reached is of the order of 100 radii of the initial source particle. In the case of atmospheric aerosols, the size range of the particulates is 0.02–2 μm, and their number density is in the range of 1000–10,000 particles/cm^3 within an altitude of 1 km.[10,11] These data suggest that an acoustic waveform is arrived at before any interference between individual source waves has occurred. Hence, the observer detects an interference pattern of acoustic waves. The individual acoustic waveform is expressed by the pressure function

$$p_0(|r_i|, t) = [\theta(t - |r_i|/c) - \theta(t - |r_{ii}|/c)] + 1/2\pi \int_{-\infty}^{\infty} P_0(\omega) e^{jwt}\, d\omega \qquad (5)$$

where $P_0(\omega)$ is the Fourier transform of $p_0(r_i, t)$ in the interval $r_i - r_{ii}$. In the general case in which the observer is positioned anywhere in the field and may have a directivity response, r_i is a three-dimensional vector in the real space. Thus, the ensemble pressure waveform due to N sources at the observer location is expressed as

$$p(t) = \sum_{i=1}^{N} p_0(r_{\text{ref}}, t) r_{\text{ref}} \frac{e^{-jkr_i}}{|r_i|} f(\alpha_i) \qquad (6)$$

where

$k = 2\pi/\lambda$

$\lambda \sim r_i - r_{ii}$

r_{ref} = reference distance from source

α_i = angle between normal to the observer plane and line from source to observer

$f(\alpha_i)$ = directivity response function

and

$$p_0(r_{\text{ref}}, t) r_{\text{ref}}/|r_i| \equiv p_0(|r_i|, t)$$

However, a detector such as a microphone used to detect the pressure waves acts as a filter and modifies the ensemble waveform. The measured signal by a microphone can be formulated as

$$P_{\text{ac}}(t) = (1/2\pi) \int_{-\infty}^{\infty} P(\omega) H(\omega) e^{j\omega t}\, d\omega \qquad (7)$$

where $P(\omega)$ is the Fourier transform of the ensemble wave function and $H(\omega)$ the microphone response function. For a population of particulates absorbing a constant amount of energy, $p_0(r_{\text{ref}}, t)$ is identical. Under such conditions, Eq. (6) can be reorganized, and $P(\omega)$ can be expressed as

$$P(\omega) = \int_{-\infty}^{\infty} P_0(r_{\text{ref}}, t) r_{\text{ref}}\, e^{-j\omega t} \sum_{i=1}^{N} \frac{e^{-jkr_i}}{|r_i|} f\, dt$$

or

$$P(\omega) = \left[\int_{-\infty}^{\infty} P_0(r_{\text{ref}}, t) e^{-jwt}\, dt \right] r_{\text{ref}} \sum_{i=1}^{N} \frac{e^{-jkr_i}}{|r_i|} f(\alpha_i) \qquad (8)$$

So, finally, one arrives at the expression

$$P(\omega) = P_0(\omega) r_{\text{ref}} \sum_{i=1}^{N} \frac{e^{-jkr_i/c}}{|r_i|} f(\alpha_i) \qquad (9)$$

That $P(\omega)$ is a product of the individual wave function Fourier transform and the sum of location-dependent terms results in considerable simplification of the numerical computations. The geometric arrangement consists of a cylindrical test cell with transparent windows at its two ends to enable the laser beam to enter and leave the cell. The laser beam propagates concentrically with the cell axis, and a microphone is located on the cell wall in the middle of the cell length. The

test cell is filled with a gas sample that contains particulates of uniform absorption cross section, which are randomly distributed in the cell volume. A schematic of this arrangement is shown in Fig. 3. In the present example, the cell has a length of 24 cm and a diameter of 15 cm. The laser beam has a diameter of 3.5 cm. The particulates absorb 0.05 erg each of the laser energy. A reference distance was set at $r_{ref} = 1$ cm. An individual waveform at the location is shown in Fig. 4. This waveform is represented by 128 points, and its temporal width is 470 ns. Its amplitude is 660 Pa.

A Fourier transform of the waveform was obtained first by using an FFT algorithm and second by using a DFT algorithm (fast and digitized Fourier transform, respectively). Fine resolution of the spectrum is needed to obtain some spectral information within the microphone response range. Microphones of spectral response that are fully compatible with this wave spectrum are not available. Piezoelectric transducers operable in gas are similarly audio frequency-limited, due to the low specific acoustic impedances of gases. Also, the farther a microphone response reaches toward high frequencies, the lower is its sensitivity. One of the highest-frequency-response microphones is Bruel & Kjaer model 4135. The use of this microphone has been assumed in the present example. Its response function is shown in Fig. 5. Its phase has been assumed constant. As seen, the response function does not extend farther than 150 kHz. If at least several points of the waveform spectrum are desired in this range, then the waveform represented by 128 points needs to be padded on both sides by zero values. Thus, having an array of 16384 points yields a frequency resolution of 16.6 kHz. This array was used as input data to the FFT. The resulting power spectrum density (PSD) is given in Fig. 6. Most of the energy lies below a frequency of 10 MHz. However, observation of the spectrum in the range of up to 10 MHz, as demonstrated in Fig. 7, shows that the energy is contributed mainly by components of frequencies greater than 150 kHz. Thus, in order to verify the FFT results below 150 kHz, and to obtain good resolution, we performed a DFT computation in the range 0–200 kHz. The results compare favorably with the FFT in the range and are shown in Fig. 8. Then, $P(\omega)$ was calculated, assuming a directivity function cosine of the angle between the normal to the microphone and the line to the source, multiplied by $H(\omega)$, and inverse-Fourier-transformed to obtain the acquired signal waveform $P_{ac}(t)$.

The inverse Fourier transform was performed using an inverse FFT algorithm with 4096 points in the frequency domain. This yields a resolution of 3 ns in the time domain. We calculated waveforms that are due to a variety of number of particulates N in the laser beam. Values of $N = 2$, 10, 100, 1000, and 10,000 were used, and the resulting waveforms are shown in Figs. 9–13, respectively. The pressure axis is relative to the ambient pressure and is given in arbitrary units mutually scaled by a common normalization factor. In Fig. 9, we can distinctly see the contribution of each of the two particulates to the pressure because the wave combination is incoherent. The individual filtered waveform is quite modified with respect to the unfiltered one, clearly because of exclusion of the major spectral contributions. We can observe that the wave arriving first at the microphone is of a greater absolute value amplitude than the last, on account of a shorter distance between the wave source location and the microphone. In Fig. 10, the combination of the wave is mostly incoherent again,

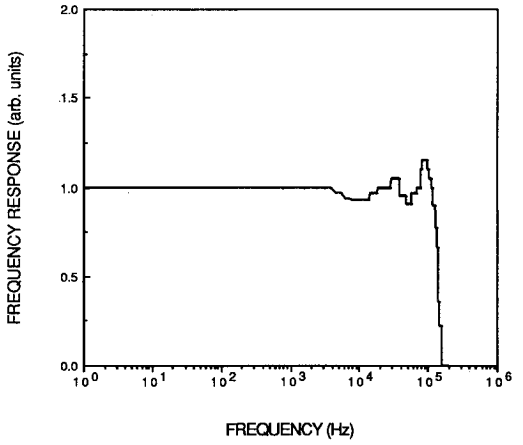

Fig. 5 Response function of Bruel & Kjaer model 4135 microphone.

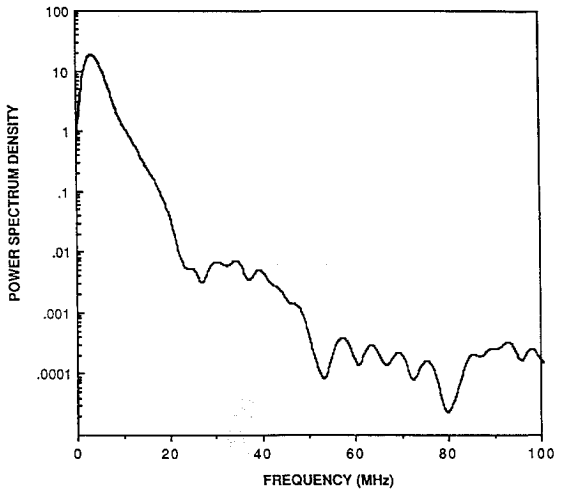

Fig. 6 Power spectrum density (PSD) by an FFT of a single acoustic wave.

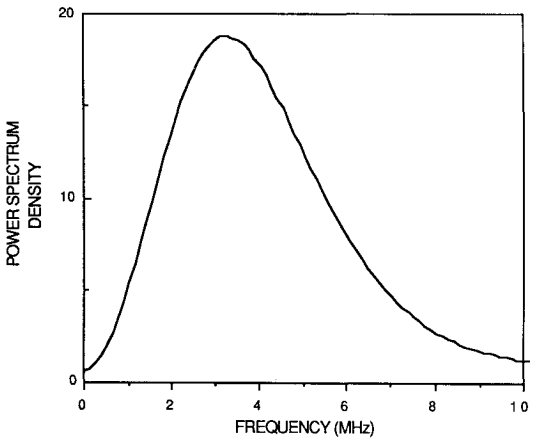

Fig. 7 PSD by an FFT of a single acoustic wave in the band of 0–10 MHz.

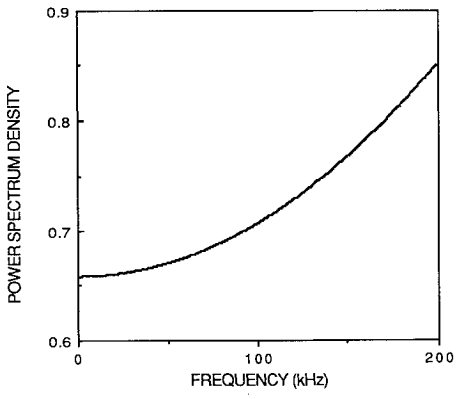

Fig. 8 PSD by a DFT of a single acoustic wave in the band of 0–200 kHz.

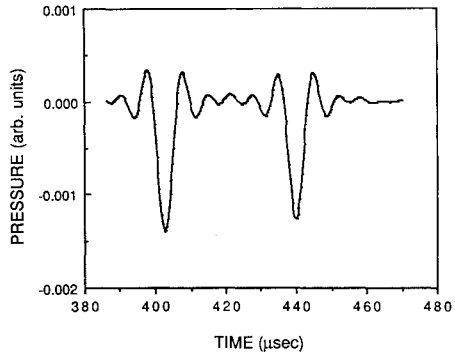

Fig. 9 Acquired signal from an ensemble acoustic wave, $N = 2$.

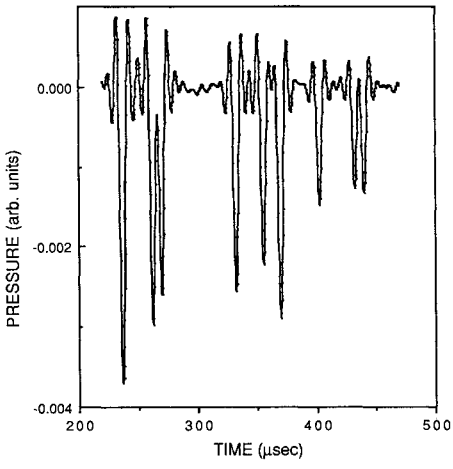

Fig. 10 Acquired signal from an ensemble acoustic wave, $N = 10$.

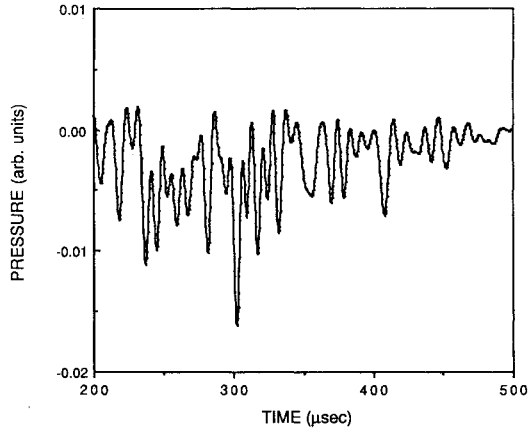

Fig. 11 Acquired signal from an ensemble acoustic wave, $N = 100$.

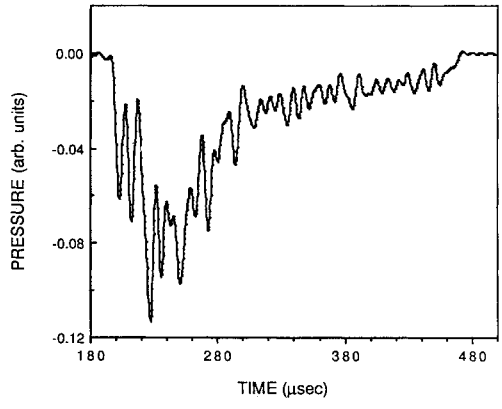

Fig. 12 Acquired signal from an ensemble acoustic wave, $n = 1000$.

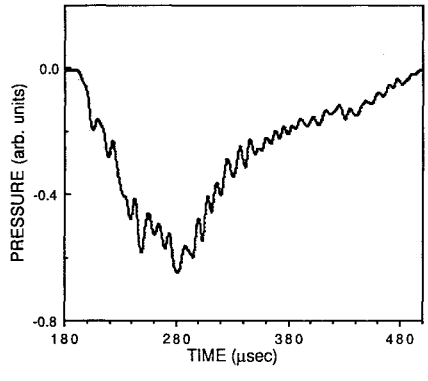

Fig. 13 Acquired signal from an ensemble acoustic wave, $N = 10000$.

and only the sixth spike, located at 370 μs, has a combined amplitude resulting from two waves. So, one should expect more coherent combinations for test cases including more particulates. Indeed, in Fig. 11, where $N = 100$, the average absolute value of the amplitude is greater than the case of $N = 10$. Further, amplitude magnification is obtained for $N = 1000$, as seen in Fig. 12. Here the combination is coherent to a greater extent, giving rise to a distinct waveform pattern. This pattern of the filtered function, or the acquired signal, has only negative values. We can explain it by observation of the individual waveform, as seen in Fig. 4. It is a bipolar signal, but its positive lobe is of a higher frequency than the negative, and the lower-frequency components superpose more coherently than the higher ones. Then there is also the effect of the microphone that acts as a low pass filter. In Fig. 13, where $N = 10{,}000$, the same pattern is preserved and the noisy high-frequency modulation is deceased. Note that the amplitude in Fig. 13 is 10 times the one in Fig. 12. Hence, the greater the number of particulates in the test volume, the more coherent and less noisy the measured signal. After a certain minimum, about $N = 1000$, the signal amplitude grows linearly with N. Some properties of the signal reflect the geometric arrangement of the test cell. The entire pulse width is slightly less than 300 μs, which corresponds to the distance between the nearest and the farthest particulates, viewed from the microphone location. The pulse full-width half-maximum (FWHM) corresponds to the laser beam diameter. Should the test cell be longer than the present value of 24 cm, the contribution of the additional wave sources to the signal would not be significant. In this test case, in which the absorbed energy is 0.05 erg per particulate, the relative amplitude of the wave at the reference location (1 cm from its source) is 660 Pa. The ordinate values of Figs. 9–13 are scaled in this test case as $1 \propto 100$ Pa. So the amplitude of the ensemble filtered wave at the microphone location for $N = 10{,}000$ is -60 Pa. Because the assumed microphone, Bruel & Kjaer model 4135, has a sensitivity of 4 mV/Pa, the output signal from the microphone in this case will have an amplitude of -0.24 V. This microphone has a noise level of 2 mPA, so that the predicted signal to the microphone noise ratio is 30,000.

IV. Conclusions

In the present study, an optoacoustic method for measuring the absorption of laser energy by particulates in gas was analyzed. If the energy absorbed by a single particulate is sufficiently high, it will generate acoustic waves. These waves initiating from many particulates will interfere and give rise to an ensemble wave that is detected by a microphone. In the course of this analysis, we have calculated the waveform

generated by an individual absorbing particulate, its spectrum and the ensemble wave spectrum, and the signal waveform measured by the microphone.

It has been shown that:

1) The individual acoustic wave depends, both in amplitude and length, only on the amount of energy absorbed by the absorbing particulate.

2) In calculating a test case in which most of the acoustic energy from absorption of 0.05 erg was filtered out by the microphone, there was a signal of a detectable amplitude. If 10,000 particulates reside in the illuminating laser beam, then the predicted signal amplitude is 240 mV, and the signal-to-noise ratio is 30,000.

3) For 1000 illuminated particulates or more, the acquired signal amplitude is proportional to the number of particulates.

4) The acquired signal waveform width corresponds to the laser beam diameter and the length of the test cell.

Appendix

We consider an iron sphere having a diameter of 3 μm to be illuminated by a pulse of laser radiation. The laser wavelength is of about 1 μm (for instance Nd:YAG laser). Its beam is collimated to a cylindrical shape, with a diameter of 3.5 cm. The laser emits an energy of 1 J/pulse. Iron has a complex refractive index of 3.22–4.18 at the wavelength of 1 rm. It follows that the sphere cross section for absorption is 60 percent of its geometric cross section.[4] Under these conditions, the spherical particulate absorbs energy of 0.05 erg.

Acknowledgments

This work is funded under MIT Lincoln Laboratory Purchase Order BX-1821, Dept. of the Air Force Prime Contract F19628-85-C-0002. The authors wish to express their thanks to Dr. S. Fulghum and G. Morales for their assistance in the computational effort.

References

[1]Tam, A. C., "Applications of Photo-acoustic Sensing Techniques," IBM Research Laboratory, San Jose, CA, Research Rept RJ(49443), March 1985.

[2]Dabora, E. K., "Energy and Power Requirements for Direct Initiation of Spray Detonations," *Proceedings of the 12th Shock Tube Symposium,* edited by A. Lifshitz and J. Rom, Jerusalem, 1979.

[3]Killinger, D. K. and Menyuk, N., "Laser Remote Sensing of the Atmosphere," *Science*, No. 235, Jan. 1987, p. 37.

[4]Kerker, M., *The Scattering of Light and Other Electromagnetic Radiation,* Academic, New York, 1969, Chap. 4.

[5]Brode, H. L., "Blast Wave from a Spherical Charge," *Physics of Fluids*, Vol. 2, No. 2, March–April 1959, p. 217.

[6]Stenberg, H. M. and Walker, W. A., "Calculated Flow and Energy Distribution Following Underwater Detonation of a Pentolite Sphere," *Physics of Fluids*, Vol. 14, Sept. 1971, p. 1869.

[7]Eidelman, S. and Burcat, A., "The Evolution of a Detonation Wave in a Cloud of Fuel Droplets: Part I, Influence of the Igniting Explosion," *AIAA Journal*, Vol. 18, Sept. 1980, p. 1103.

[8]Boris, J. P. and Book, D. L., "Solution of Continuity Equations by Method of Flux Corrected Transport," *Methods of Computational Physics*, Academic, Vol. 16, 1976, pp. 85–129.

[9]Book, D. L. et al., "Simulation of Complex Shock Reflections from Wedge in Inert and Reactive Gas Mixtures," *Proceedings of the 7th International Conference on Numerical Methods in Fluid Dynamics*, Springer-Verlag, New York 1980, pp. 84–90.

[10]Driscoll, W. G., (ed.), *Handbook of Optics,* McGraw-Hill, New York, 1978, Chap. 14.

[11]Devara, P. C. S. and Raj, P. E., "Bistatic Laser Radar System for Remote Sounding of Aerosols in the Lower Troposphere," presented at the Conference on Lasers and Electro Optics, Baltimore, MD, 1987.

[12]Resch, F. J. and Abel, R., "Spectral Analysis Using Fourier Transform Techniques," *International Journal for Numerical Methods in Engineering*, Vol. 9, 1975, p. 869.